Soil Moisture Active/Passive (SMAP) L-band Microwave Radiometer Post-Launch Calibration Revisit: Approach and Performance

Jinzheng Peng[1,2], Sidharth Misra[3], Jeffrey R. Piepmeier[1], Simon H. Yueh[3], David M. Le Vine[1], Emmanuel P. Dinnat[1,4], R. Scott Dunbar[3], Priscilla N. Mohammed[1,5], Steven K. Chan[3], Thomas Meissner[6]

[1]NASA Goddard Space Flight Center, Greenbelt, MD 20771 USA
[2]Universities Space Research Association, Columbia, MD 21046 USA
[3]Jet Propulsion Laboratory, California Institute of Technology, Pasadena, CA 91109 USA
[4]Chapman University, Orange, CA 92866 USA
[5]Morgan State University, Baltimore, MD 21251 USA
[6]Remote Sensing Systems, Santa Rosa, CA 95401 USA

Abstract— The SMAP microwave radiometer is a fully-polarimetric L-band radiometer flown on the SMAP satellite in a 6 AM / 6 PM sun-synchronous orbit at 685-km altitude. After the SMAP L1B_TB data product version 4 was released in 2018, the radiometer has undergone further calibration and validation. The goal is to reduce the difference between antenna temperature (TA) of ascending and descending orbits during the eclipse, and to reduce the dips in the calibration drift over the Cold Sky (CS) during the eclipse seasons in 2017 and 2018. The post-launch calibration algorithm has been revisited by retrieving all of the calibration parameters simultaneously with two different options for the hot calibration source (the global ocean, or the radiometer internal reference load). The performance of the two options are compared here. The option with the radiometer internal reference load has been chosen by the SMAP science team for data release version 5. In addition, a correction offset is applied to the input signal to account for offsets during the early-mission stages with the SMAP SAR transmitter operating alongside the radiometer.

I. INTRODUCTION

The Soil Moisture Active Passive (SMAP) mission was launched on Jan. 31, 2015 in a 6 AM/ 6 PM (descending/ascending) sun-synchronous orbit at 685 km altitude with the objective of measuring soil moisture and free/thaw globally [1]. The SMAP L-band microwave radiometer is a fully polarimetric L-band radiometer (1.4 GHz) operating with a bandwidth of 24 MHz. The radiometer uses a combination of noise-diodes and Dicke-loads for internal calibration with a design similar to that used by the Jason, SMOS (Soil Moisture and Ocean Salinity) and Aquarius series radiometers [2, 3, 4]. The radiometer ground processing algorithm converts raw counts to antenna temperature (TA) and the Earth's surface brightness temperature (TB). The algorithm includes advanced Radio Frequency Interference (RFI) detection with the aid of special flight hardware to remove corrupted L-band measurements [5, 6, 7]. These TB values are used with other ancillary data to retrieve soil-moisture products on a 40km global grid. The radiometric uncertainty requirement for the SMAP radiometer is 1.3 K with a calibration drift of less than 0.4 K/month in order to measure soil-moisture with a volumetric fraction uncertainty of less than 0.04 m^3/m^3 [1].

The SMAP radiometer has successfully operated in space since it was fully deployed two months after launch. Two data versions (3 and 4) have been released to the public for science activities with different calibration approaches, and both of them satisfy the requirements. The radiometer L1B data product version 3 was released in April 2016. The performance of version 3 during the first year on orbit is reported in [8], and the post-launch calibration and part of its validation are described in [9]. The reflector emissivities measured before launch were used. The antenna mainbeam gain and the equivalent brightness temperature of the noise diode were then calibrated one after another. Validation results for data product version 3 show that the SMAP antenna temperature is 2.6 K warmer than the reference forward model simulation over CS, and that the averaged SMAP TB is 2.6 K colder over land than the averaged SMOS TB (compared at the top of the atmosphere for the two L-band satellites with co-located and concurrent measurements), including the update of the reflector's thermal model. Also, there is downward dip in the calibration over the global ocean during eclipse seasons [9]. In order to remove these biases and mitigate the calibration drift, the SMAP radiometer was re-calibrated, and the corresponding data product, version 4, was released in 2018 [10].

In the calibration for data product version 4, the reflector emissivity was calibrated first by three different research teams using different approaches and datasets, and the results agreed within 0.5% for the reflector loss [10]. Then the other calibration parameters (antenna gain, equivalent brightness temperature of the noise diode, and the offset to the equivalent brightness temperature of the reference load) were concurrently recalibrated (i.e. multiple calibration parameters were calibrated simultaneously). The validated results are shown in [10, 11].

Although the data product version 4 satisfies the soil moisture science requirements, two calibration issues remain: (1) there is a maximum of 0.7 K difference in the calibration drift over the global ocean between ascending and descending orbits, and (2) Dips of 0.4 K magnitude in the calibration drift over CS in 2017 & 2018 but not in the

previous years. These were reported after the release of data version 4 and appeared during the summer eclipse seasons (i.e. from May to August). In addition, the brightness temperature increased by about 3 K over land surfaces compared with version 3 datasets. This impacted the level 2 soil moisture retrieval, resulting in the need to make an ad-hoc adjustment of 2% to the effective land surface temperature to reduce a dry bias in the soil moisture retrieval. Analysis shows that these issues may be caused by the following three factors: 1) inaccuracy in the reflector temperature model for the eclipse period; 2) bias in the estimated reflector emissivity; 3) bias in the ocean Geophysical Model Function (GMF) [12]. Based on this analysis, the SMAP radiometer calibration has been revisited to investigate the causes and to improve data quality.

In the next sections, the revisited calibration algorithms for the SMAP radiometer L1B and the associated data products are presented, including the calibration approach for correcting the TA bias due to the Synthetic Aperture Radar (SAR) transmitter power-down and the radiometer internal drift during the first few months. The calibration results are evaluated at both TA and TB levels in Section III. Lastly, the results will be discussed, and conclusions will be made for the data product version 5.

II. Radiometer Calibration Algorithm Revisit and Result

In the previous two calibration algorithms for the SMAP radiometer, the calibration was performed in sequential steps [9, 10]. The SMAP radiometer calibration includes determining the equivalent noise temperatures of the noise diode and the reference load (T_{ND} and T_{ref}), correcting the antenna pattern, characterizing the RF front-end loss, and the antenna system loss (feedhorn aperture cover and reflector emissivity). Calibration of these parameters directly impact the gain and offset of the antenna temperature measurements. The calibration algorithm is revisited here using an approach that retrieves all of the calibration parameters concurrently (or simultaneously) to obtain an optimal solution. The calibration algorithm are run with two options for the hot calibration targets. Their performance is compared and one chosen for the next L1B_TB data release.

Similar to the calibration for data release version 4 [10], the calibration remains divided into 2 phases: (1) Prior to July 7, 2015 when the radar was operational; and (2) After July 7 when the radar stopped transmitting. The calibration for Phase 2 is performed first because the radiometer is stable.

A. External Calibration/Validation Targets

The primary external targets for SMAP calibration/validation are CS (cold target, e.g. Fig. 3b in [9]) and the global ocean (hot target, e.g. Fig. 1 in [10]). In addition, the Amazon rainforest and the African continent (unpolarized targets) are used for the special CS calibration to augment the post-launch calibration. Besides the monthly CS calibration with a pitch angle of 110° (CS110) over ocean, the special CS calibrations have pitch angles of 180° (CS180) and 35.5° (CS35) over the Amazon rainforest and the African continent, respectively. The SMAP spacecraft attitude including ground track and antenna pointing directions with different pitch angles are shown in Fig. 2 in [9, 10], whereas Fig. 2b in [10] shows nadir pointing when the antenna scan angle is 0°. Note: The sign of the pitch angles is negative but omitted for convenience.

There are no sensors on the reflector and its temperature is modeled. Figure 1a shows an example of the modeled reflector temperatures on the fifteenth day of March, June, August, and December of 2016. Beyond the summer eclipse season, the reflector temperature ranges from 103 ℃ to 125℃, while during the eclipse season (e.g. Jun 15, 2016), it has a much broader range from 15℃ to 136℃ and a much larger temperature difference between ascending and descending orbits. This can cause the difference in the calibration drift over the global ocean between ascending and descending orbits during the summer eclipse season if the reflector loss is not accurately calibrated.

In the calibration for version 4 data, the time span of the global ocean and CS data used for Phase 2 calibration is about one year (from August 2015 to July 2016). During this period, the reflector temperature during the CS calibration is within the range [106℃ 120℃]. During the summer eclipse seasons, CS110s were performed over the southern hemisphere in 2016 and over the northern hemisphere in 2017 and 2018. For the latter, the corresponding reflector temperatures are higher than 120℃ as shown in Figure 1b. The reflector temperature during the CS calibration should have a dynamic range as wide as possible (to cover all possibilities). Consequently, the global ocean and normal CS calibration data during the eclipse seasons of 2017 and 2018 are included in the revisited calibration for Version 5.

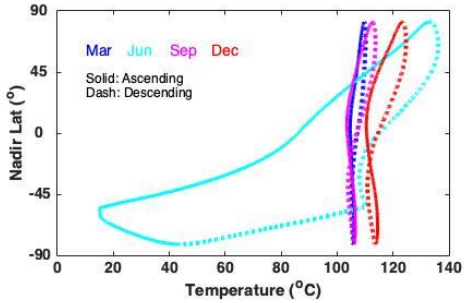

(a)

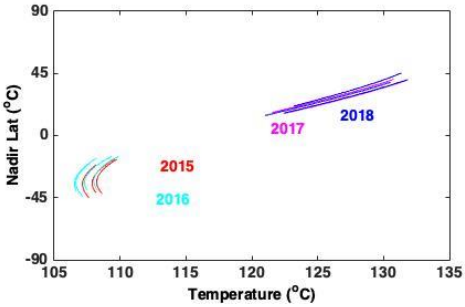

(b)

Figure 1. Reflector temperatures. (a) The reflector temperature on the 15th of March, June, September and December in 2016. (b) The reflector temperature with spacecraft pitch angle 110° during the eclipse seasons in 2015~2018.

B. *Calibration Algorithm Revisit for Phase 2*

In the revisited calibration, there are 20 CS calibration maneuvers for the Phase 2 calibration. The CS data are averaged over the time span (e.g. 6.02 ± 0.06 minutes duration for CS110 and 10.14 minutes duration for CS180) of the CS look. When the global ocean is used as an external hot calibration target, the data over the global ocean are separated into ascending/descending half orbits before averaged over a 3-day time span. The selected three days for each averaging are the day of the CS calibration plus one day before and one day after. When the radiometer internal reference load is used as a hot calibration target, its brightness temperature is assumed to be well-known (i.e. no bias or zero correction) due to that there is a temperature measurement for the reference load and the RF front-end components have been calibrated before launch.

Two algorithms for the two calibration options are described below.

1) Option 1: Global Ocean as the Hot Calibration Target

The calibration parameters in Option 1 are the same as those in the calibration algorithm for the SMAP radiometer L1B data product version 4 [10]. For the polarization channels V and H, the relationship among the residual calibration bias δT_A and the corrections to all of the calibration parameters (reflector loss, antenna gain, the equivalent noise temperatures of the noise diode and the reference load) are given by (see Equation (A.8) in appendix)

$$\delta T_A = \delta T_{A,0} + L_{RF}\left(C_r \delta T_{ND} + \delta T_{ref}\right) + T_{A,exp,0}\left\{1 - \frac{1+\alpha\delta_G}{f_L}\right\} - \frac{T_{phy,rfl}}{L}\left\{L - \frac{1}{f_L}\right\} - B_T \quad (1)$$

where $\delta T_{A,0}$ is the calibration bias before the calibration parameters are adjusted. $T_{A,exp,0}$ is the expected TA without antenna gain and reflector loss corrections. L_{RF} is the loss of the SMAP RF front-end and, because it depends on temperature, it varies with observations. $C_r = \frac{C_{ant} - C_{ref}}{C_{nd}}$, and $C_x (x = ant, ref, nd)$ are radiometer measurements when looking through the antenna and at the calibration sources. $\delta T_{ND}, \delta T_{ref}$ and δ_G are the corrections to T_{ND}, T_{ref} and antenna gain, respectively. α is a scale factor that reflects the true antenna temperature change due to the normalization of the antenna pattern after the antenna mainbeam is adjusted, and it is obtained by using simulation. $T_{phy,rfl}$ is the ambient temperature of the reflector. f_L is a scale factor for correcting the pre-launch reflector loss L. B_T is a bias at the TA level and an additional subscript (e.g. GO or CS) is used to identify the bias is for the global ocean or CS. For the global ocean, $B_{T,GO}$ is the bias at the TA level for the H-polarization ocean roughness model [12] in normal science mode, and it is used to minimize ΔT_A for the nadir-looking measurements:

$$\Delta T_A = \left(T_{A,v} - T_{A,sim,v}\right) - \left(T_{A,h} - T_{A,sim,h}\right) \quad (2)$$

where $T_{A,x}$ (x=v, h) is the TA measurement for x-polarization, and $T_{A,sim,x}$ (x=v, h) is the simulated TA for x-polarization. Subscript '*sim*' instead of '*exp*' is used here to identify the special case of nadir-looking simulation. For CS, $B_{T,CS}$ is the bias at the TA level to minimize the residual error in ΔT_A after calibration coefficients were updated.

For each polarization, there are at least 7 independent TA measurements (CS180 over ocean, CS180 over Amazon, CS110 during non-eclipse season, CS110 over Northern hemisphere during eclipse season, CS110 over Southern hemisphere during eclipse season, ascending and descending measurements over ocean in normal science mode). In addition, there are two nadir TA measurements (one over ocean and one over land). Therefore, there are at least 16 independent TA measurements.

In Equations 1 & 2, there are 10 unknowns (4 corrections for each polarization, plus the ocean TA model bias $B_{T,GO}$ at H-polarization and the CS TA model bias $B_{T,CS}$ which has equal magnitude but opposite sign for V and H polarizations) which are less than the number of independent measurements, so the Equations 1 & 2 are over-determined. The solutions of the unknowns are unique, and they can be obtained by using the iterative Newton-Raphson method. The results are listed in Table 1. Note: An ad-hoc bias '-0.15 K' has been added to the ocean TA model at V-polarization to keep the TB over land the same as that in Version 4. Without this ad-hoc bias, the TB over land will be about 0.5 K higher.

Table 1. Correction in Calibration Coefficients for Phase 2, Option 1

Pol.	δT_{ND}	δT_{ref}	f_L	
V	-0.13 K	2.81 K	1.0071	
H	0.84 K	2.76 K	1.0070	
Pol.	δ_G	$1+\delta_G$	$B_{T,CS}$	$B_{T,GO}$
V	-0.0013	-0.013 dB	+0.32 K	-0.15 K
H	-0.0044	-0.044 dB	-0.32 K	-0.74 K

The negative sign in δ_G means that the antenna gain needs to be reduced from the gain determined prior to launch. This is consistent with the antenna gain correction in Version 4.

2) Option 2: Reference Load as the Hot Calibration Target

The reference load inside the radiometer is used as the hot calibration target in this option. The brightness temperature of the reference load (Equation 4a in [8]) is assumed to be modeled well, and additional correction (i.e. δT_{ref} in Option 1) is not needed. Therefore, Equation 1 is simplified as

$$\delta T_A = \delta T_{A,0} + L_{RF} C_r \delta T_{ND} + T_{A,exp,0}\left\{1 - \frac{1+\alpha\delta_G}{f_L}\right\} - \frac{T_{phy,rfl}}{L}\left\{L - \frac{1}{f_L}\right\} \quad (3)$$

For each polarization, there are at least 5 independent TA measurements (CS180 over ocean, CS180 over Amazon, CS110 during non-eclipse season, CS110 over Northern hemisphere during eclipse season, CS110 over Southern hemisphere during eclipse season). Since the model TB of

the reference load is assumed to be well-known and the correction to the reflector loss factor is assumed to be the same for both V- and H-pols, there are 5 unknowns in the calibration parameter list. Therefore, Equation (3) is also over-determined. Using the iterative Newton-Raphson method, the corrections can be solved and are listed in Table 2

Table 2. Correction in Calibration Coefficients for Phase 2, Option 2

Pol.	δT_{ND}	δ_G	$1+\delta_G$	f_L
V	-2.22 K	-0.0009	-0.004 dB	1.0040
H	2.20 K	-0.0037	-0.016 dB	

As with Option 1, the negative sign in δ_G means that the antenna gain needs to be reduced from the gain determined prior to launch. This is consistent with the antenna gain correction in Version 4.

The corrections to the same calibration parameter are different for Options 1 and 2. The difference is expected because of the different hot calibration targets. However, both options result in increment of the reflector loss and decrement of the antenna gain, and this result is consistent with that of the calibration for Version 4.

3) Performance comparison between Options 1 & 2

For each option, two years of data have been generated using the updated calibration coefficients. The calibration drift over global ocean and CS are shown in Figure 2 and Figure 3 for Options 1 & 2, respectively.

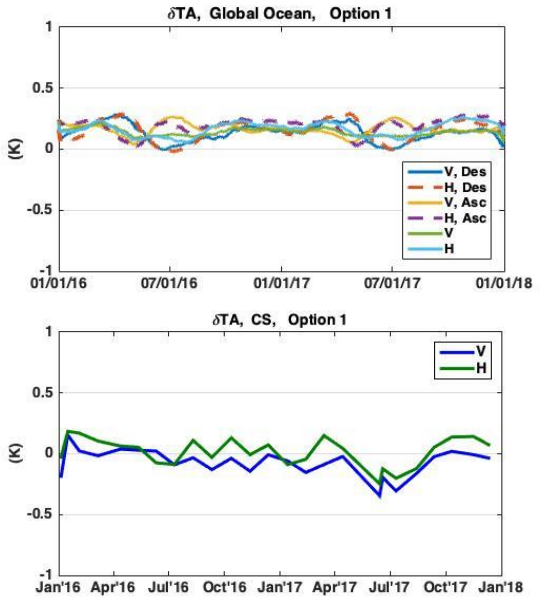

Figure 2. Calibration drift for Option 1. (a) over the global ocean; (b) over CS.

Their performances are listed in Table 3.

Sixteen days of data during Feb 03~18, 2016 (SMAP orbit repeats every 8 days) are used to check the change of TB over the Earth's land compared to the TB data of the previous versions. The TB data over land are chosen with that both water fraction and sea ice fraction are less than 0.001. The results are shown in Table 4.

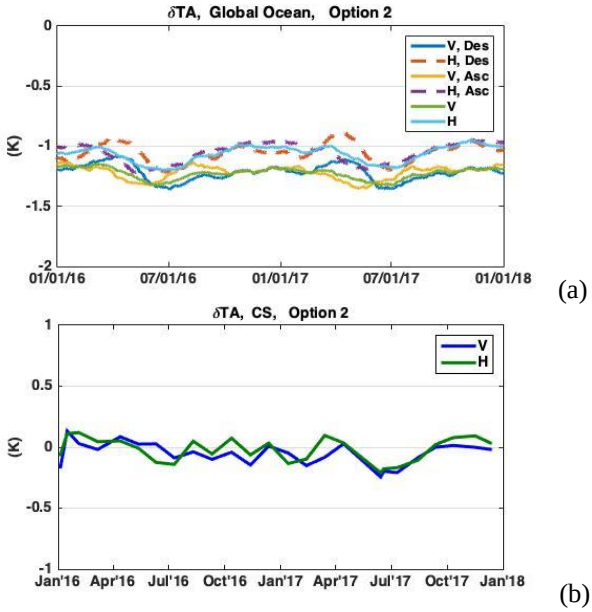

Figure 3. Calibration drift for Option 2. (a) over the global ocean; (b) over CS.

Table 3. Calibration Drift Performance Comparison

Target	Parameters	Option 1	Option 2
global ocean	Drift rate (abs)	0.03 K/year	0.02 K/year
	Bias*	0.14 K (v) 0.16 K (h)	-1.22 K (v) -1.05 K (h)
	Asc & Des diff	0.26 K	0.25 K
CS	Drift rate (abs)	0.06 K/year	0.05 K/year
	Bias*	-0.07 K (v) 0.01 K (h)	-0.05 K (v) -0.03 K (h)
	Dip magnitude	0.25 K	0.18 K

* Known bias (e.g. $B_{T,GO}$ and $B_{T,CS}$) is removed from results listed in this table.

Table 4. Change of TB over Land

	Option 1		Option 2	
	V	H	V	H
Ver. 3	2.97 K	3.59 K	0.02 K	1.01 K
Ver. 4	0.10 K	0.27 K	-2.85 K	-2.31 K
SMOS*	1.0 K	1.6 K	-2.2 K	-1.3 K

Note: Positive sign means the TB of Option x (x=1 or 2) is higher than the TB of Ver. y (y=3 or 4) or SMOS.

* Estimated value for TB change over land within latitude $\pm 40°$.

In addition, the TB differences between SMAP and SMOS data (Version 620) are shown in Table 4. The results of the TB inter-comparison between SMAP Version 4 data and SMOS Version 620 in [10] are used as the reference to derive the difference and shown here.

Option 1 requires an addition of 2.81 K for V-pol and 2.79 K for H-pol to the TBs of the reference load. These values seem too large to be reasonable. Also, the correction to the reflector loss of Option 1 is larger than that of Option 2. Using the measurements of the reflector loss before launch as references, the correction to the reflector loss of Option 2 seems to be more trustworthy.

Option 2 has a lower TB over land than Option 1. This is beneficial to reduce the ad-hoc adjustment, 2% in Version 4, of the effective land surface temperature used in the level 2 soil moisture retrieval, so it is better consistent for soil emissivity models in use by SMAP Level 2 data product. Furthermore, Option 1 uses the global ocean as the hot external calibration target, but the bias on the oceanic Geophysical Model Function (GMF) [12] is unknown. In addition, the performance of TA drift is slightly better for Option 2. Due to the above reasons, Option 2 is chosen for the SMAP radiometer L1B_TB calibration for the next release.

C. *Calibration Algorithm Revisit for Phase 1*

Phase 1 and Phase 2 are separated on Jul 07, 2015 when SAR stopped transmitting. During Phase 1 (prior to July 07, 2015), the radar transmitter was on in general. It was powered off several times for the radar RFI survey and a flight software upgrade. The radiometer's measured TA was drifting for the first two months in Phase 1 and then stabilized thereafter. Besides the measured TA drift, there was a drop larger than 1 K in the measured TA when the radar transmitter was turned off [9]. The measured TA change can be due to 1) noise from the SAR transmitter within the radiometer receiving frequency band or 2) the ambient temperature change.

1) *Impact of the Radar Transmitter on the Radiometer TA measurements*

The radar transmitter was powered off for 10 days (April 03~13, 2015) for the radar RFI survey. The ambient temperature of the radiometer decreased by about one degree due to the heat dissipation from the transmitter. In the middle of this SAR off period, the radiometer's ambient temperature was raised about 6℃ to 28℃ (as shown in Figure 4) for 4 days by active thermal control.

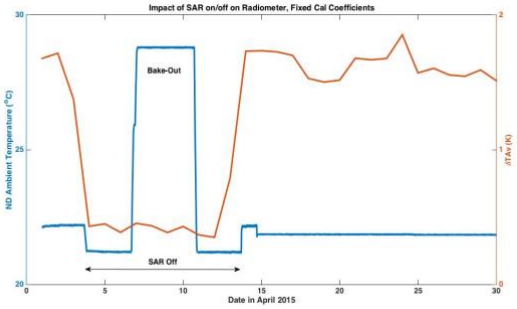

Figure 4. Radiometer calibration drift over ocean vs radiometer temperature in April 2015. The blue line is the ambient temperature of the internal noise source. The orange line is the radiometer calibration drift over ocean.

During the 10-day RFI survey period in April 2015, the radiometer was stable even though the radiometer's ambient temperature changed significantly on April 6 & 10, while the ambient temperature change was much smaller on April 13 when the transmitter was on. This evidence shows that the TA measurement's step change (>1 K over ocean) is not due to the impact of ambient temperature (the radiometer's internal calibration has corrected the impact of the radiometer's ambient temperature change). Therefore, the cause of the TA change is due to the radar transmitter. When the radar transmitter was on, the noise from the transmitter was amplified and components within the radiometer frequency band could be detected by the radiometer. This change can be treated as a fixed positive bias to the input. When the calibration coefficients T_{ND} and T_{ref} obtained from Phase 2 are used to get the calibrated TA, the fixed positive bias needs to be deducted. For algorithm convenience, a fixed negative offset can be added to T_{ref} when the transmitter is on. The negative offset (-1.16 K for V-pol and -1.26 K for H-pol) will keep the calibrated TA stable around Jul 07, 2015.

2) *Calibration Drift Removal*

After the radiometer was powered up on Mar 31, 2015, the radiometer's measured TA was drifting compared to the ocean L-band GMF model [12], shown in Figure 5(a). The drifts were about 0.31 K/month for V-pol and 0.39 K/month for H-pol for the first two months, and the radiometer is stable thereafter [9]. During the calibration phase, the antenna gain and reflector loss are from the calibration of Phase 2. As described in the above section, T_{ref} is changed depending on the SAR transmitter on/off status. Then CS is used for calibrating the equivalent noise temperature of the noise source for the days with CS maneuvers performed.

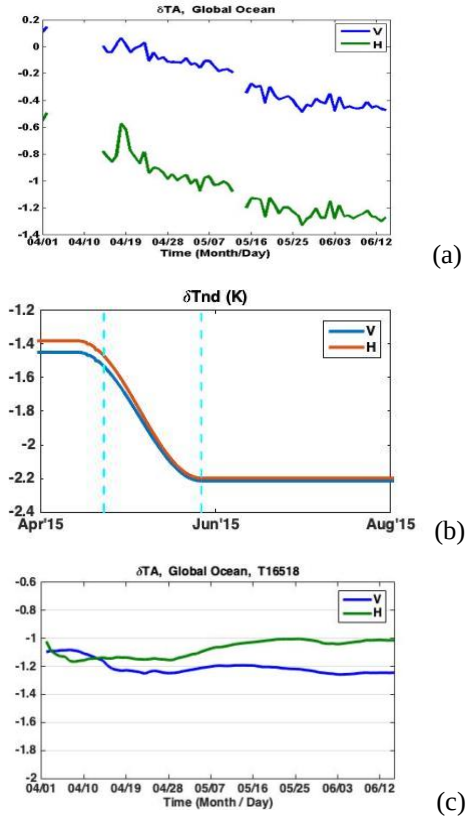

Figure 5. Radiometer TA drift. The unit of y-axis is Kelvin. (a) Before drift correction; (b) The Correction to T_{ND} for removing radiometer TA calibration drift. The two vertical dashed lines show the dates when the 1st and 2nd CS maneuvers were performed; (c) After drift correction. Biases in δT_A are matched to the biases during the SAR-off era.

The CS maneuver was performed monthly. In order to remove TA drift in the first two months, the TB of the internal noise source was modeled as a quarter of the cosine function with the highest value on Apr 17, 2015 and earlier, and the lowest value on May 27, 2015 and after. For the following reasons, the value of T_{ND} on and before Apr 17, 2015 is set to be constant: 1) The first CS maneuver was performed on Apr 27, 2015; 2) TAs from Mar 31 to Apr 17 are slightly increasing, so it is more reasonable to set T_{ND} constant instead of decreasing. The final corrections to T_{ND}s are shown in Figure 5(b).

The residual calibration drift over global ocean is shown in Figure 5(c), and its uncertainty is 0.05 K for V-pol and 0.07 K for H-pol. The biases in δT_A over the global ocean are around -1.22 K for V-pol and -1.05 K for H-pol, which are matched with the biases in the calibration drift over the global ocean after July 7, 2015; they are most likely due to the unknown bias in the ocean L-band GMF model.

III. VALIDATION AND PERFORMANCE

The calibration coefficients using the approach in Section II are validated at the TA level and the TB level. At the TA level, the radiometer data product is validated by using 1) the TA difference between the V- and H-pol channels during the nadir-looking maneuver over both land and ocean; 2) the calibration drift over the two calibration/validation targets (CS and the global ocean). At the TB level, the L1B_TB data product is validated by the seasonal variation of the TB and the TB difference between V- and H-polarizations over the Amazon. In addition, the changes in TB over the Earth's surface (land and ocean) compared to Versions 3 & 4 are also shown for SMAP radiometer L1B_TB data user's convenience.

A. TA validation and performance

1) TA difference between V- and H-pol channels during the nadir-looking maneuver

The special orbital maneuvers performed with a fixed pitch angle of 35.5° produce nadir pointed observations. These observations were used in the calibration equation for Version 4 [10] and Option 1 described in Section II.B.1 to address polarization biases produced due to potential differences in the V/H polarization reflector losses. In the calibration revisited data product version 5, an implicit assumption is made that the reflector losses are the same for both polarizations. As a result, the special nadir observation data is used as a validation set for the new calibration. This assumption has made a correlation between the two polarization channels. Therefore, the other correlation between the two polarization channels (i.e. TA difference in the V/H polarization during nadir-looking) can be used to validate the calibration. As with Version 4, TA data within ±5 degrees of nadir pointing are used to compute the TA difference between the V- and H-polarizations over both land and ocean [10]. The TA differences are -0.10 K over land and -0.47 K over ocean. This TA difference is small for soil moisture retrieval since the sensitivity of TB to soil moisture is about -2.5 K/0.01m^3m^{-3} for a 40° incidence angle and for low vegetation regions [13]. The impact on the sea surface salinity retrieval might be larger due to relative lower sensitivity (e.g. 0.5 K/psu [12]) and it needs further investigation.

2) Calibration drift over the Global Ocean and CS

The calibration drift over the global ocean by the end of December 2020 is shown in Figure 6(a). The residual biases in the calibrated TA are -1.22 K for V-pol and -1.04 K for H-pol, and the uncertainty is 0.05 K for V-pol and 0.07 K for H-pol. The long-term calibration drifts are -0.003 K/year for V-polarization and 0.016 K/year for H-polarization over the global ocean. The small variation over the global ocean is most likely due to model and ancillary data inaccuracy.

The calibration drift over CS by the end of December 2020 is shown in Figure 6(b). The biases are closed to zero and the uncertainty is 0.09 K for V-polarization and 0.11 K for H-polarization. The long-term calibration drifts are -0.016 K/year for V-polarization and 0.001 K/year for H-polarization over CS.

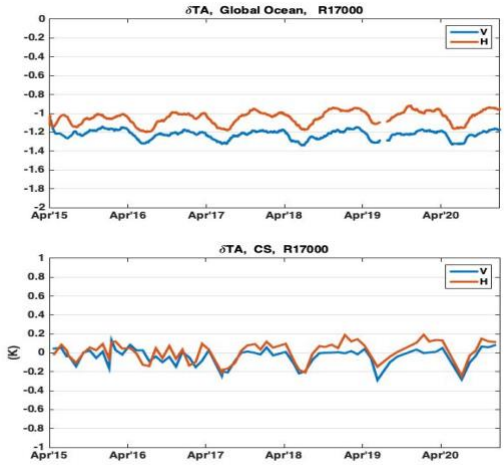

Figure 6. Residual biases or calibration drift in the calibrated TA of Version 5. (a) over the global ocean; (b) over CS.

The results are consistent with those listed in Table 3, and they show that the radiometer has been stable in the past years. In addition, the performance of the re-visited calibration coefficients is also demonstrated and validated.

B. TB validation and performance

1) TB Change over Land Compared to Versions 3 & 4

The histogram of TB differences between Version 5 and the previous versions over land are shown in Figure 7. Similar to the data used for Section II.B.3, sixteen days' data over the time period of Feb 03~18, 2016 (SMAP orbit repeat every 8 days) are used. The data with ice fraction larger than 0.001 within a given footprint are excluded. Water fraction is required to be less than 0.001 for land and larger than 0.999 for ocean. In Figure 7, the solid line includes global data, while the dashed line only includes data within latitude ±40°. The water fraction and ice fraction used in the processing are from the L1B_TB data files.

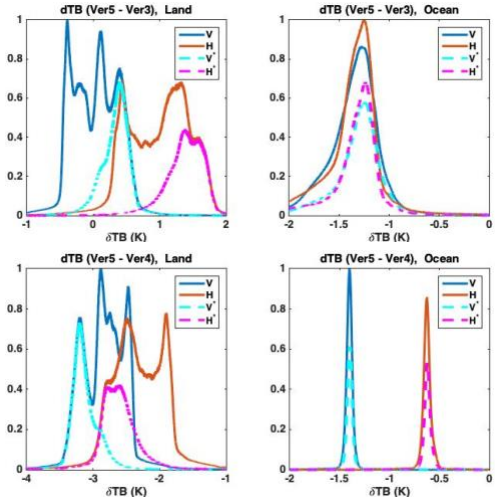

Figure 7. TB difference between Version 5 and the previous versions. (a) Version 5 vs Version 3; (b) Version 5 vs Version 4. Note: Solid line for all latitude included, and dash line for latitude within ±40°

For land, the mean TB changes without latitude constraint are listed in Table 4 labeled 'Option 2'. When data within latitude ±40° are selected, the histograms of the TB change since these data have narrower distributions and the absolute means of the TB change increase by approximately 0.3 K since the TBs close to the Equator are higher.

Over ocean the mean TB changes between Version 5 and Version 3 are about -1.35 K for both polarizations. These changes are within expected values. The SMAP antenna temperature is 2.6 K warmer than the reference forward model simulation over CS for both V- and H-polarizations, and the global ocean is used to calibrate the equivalent noise temperatures of the noise diode in Version 3. In Version 5, CS has been used as the cold calibration target and there is no bias in the calibration drift over CS. This means that the SMAP antenna temperature over CS is reduced by 2.6 K in Version 5 compared to Version 3. The SMAP TAs and TBs over the global ocean are also reduced correspondingly.

Over ocean the mean TB changes between Version 5 and Version 4 are -1.40 K and -0.62 K for V- and H-polarizations, respectively. CS is used as the cold calibration target in both Versions 4 and 5. The global ocean is used as the hot calibration target in Version 4 resulting in a correction to T_{ref} of 3.18 K and 3.29 K for V- and H-pol, respectively, while there is no correction to T_{ref} in Version 5. As a result, the TBs in Version 5 are lower than the TBs in Version 4.

With ocean data constraint within latitude ±40°, the mean TB changes are almost the same as those without latitude constraint for the comparison between Version 5 and the previous two versions. This may be a result of the exclusion of the ocean with sea ice at high latitudes. In addition, the TB changes over ocean have narrower distributions than that over land because the TBs over land have a wider range than the TBs over ocean.

2) TB Difference between V- and H-polarizations

The Amazonian forest has a dense canopy and is treated as a hot blackbody calibration target [14, 15], where the TB difference between V- and H- polarizations is expected to be small. Therefore, the Amazonian forest is used for TB validation for the data product Version 5.

The Amazon region used for validation by the SMAP radiometer is the intersection (green in Figure 8) of the regions used by the Aquarius radiometer and the Aquarius scatterometer. The Aquarius radiometer used a rectangular area [15], while the Aquarius scatterometer used a polygon region with an area inside excluded [16] due to much lower vegetation cover (within the area in the center of the green area in Figure 8).

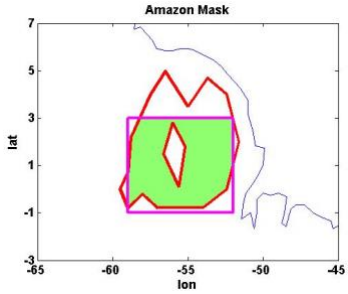

Figure 8. Amazon mask. Green region is used by the SMAP radiometer. The rectangular region enclosed by the magenta line is used by the Aquarius radiometer, and the region between the two red polygon lines is used by the Aquarius scatterometer. The coastline is in blue.

The monthly averaged TBs of the Amazon are shown in Figure 9. Seasonal signatures are observed with maximums in the summer and minimums in the winter. The mean emissivities of the Amazon area are 0.939 and 0.934 for V- and H-polarization, respectively, with a standard deviation of 0.009. It is demonstrated that the Amazonian forest cannot be used as a black body because that the L-band signal can penetrate dense vegetation and forest.

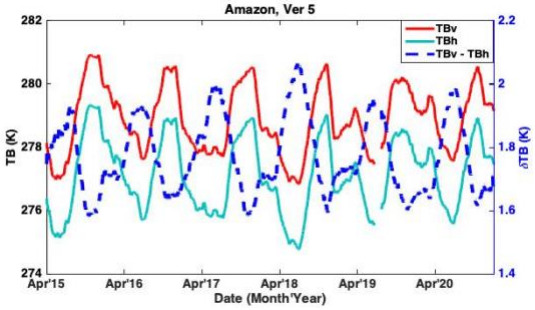

Figure 9. TBs of V- and H- polarizations and their TB differences over the Amazon.

The TB difference between V- and H-polarizations is shown in Figure 9 (dashed curve). The mean TB difference is 1.77 K. A small seasonal signature in the difference is observed with a peak-peak value of 0.4 K and a standard deviation of 0.12 K. The seasonal signature is opposite in phase to that of TBs.

IV. CONCLUSION

The SMAP radiometer's calibration has been revisited for the L1B data product version 5 based on the feedback from Level 2 soil moisture retrieval and existing issues in the L1B data product version 4. Two options with different hot calibration sources (the global ocean, the radiometer's reference load) are evaluated for the SMAP SAR-off era. For each option, all of the calibration parameters (T_{ND}, reflector loss factor, the antenna gain, and T_{ref} for the option with the global ocean as hot calibration source) are retrieved simultaneously. The two calibration options result in similar calibration drift performances with requirements satisfied and similar TA difference between ascending and descending orbits, but the two calibration options lead to different TBs of the Earth's surface. For the option using the global ocean as the hot calibration target, the globally averaged TB of the Earth's land surface is similar to that of Version 4. For the option using the radiometer's reference load, the globally averaged TB of the Earth's land surface is 2.95 K and 2.58 K lower for V- and H-polarization, respectively.

Since there might be unknown biases in the ocean GMF model used by the SMAP radiometer calibration and the relatively lower TB over land has better consistency for soil emissivity models in use, the calibration option using the radiometer's reference load is chosen for the SMAP radiometer L1B_TB data of Version 5. For the SMAP SAR-on era, T_{ND} was adjusted to remove the calibration drift for the first two months and a fixed bias was added onto the modeled TB of the reference load to remove the impact of the transmitter noise within the radiometer receiving frequency band when the SMAP SAR was on.

The long-term calibration drifts (absolute value) of Version 5 are not larger than 0.016 K/year over either the global ocean or CS with the residual uncertainty better than 0.11 K (rms). Validations show that 1) there are biases (-1.22 K for V-pol and -1.04 K for H-pol) in the calibration drift over the global ocean; 2) the TA difference between the V-polarization and H-polarization are -0.10 K over land and -0.47 K over ocean when the radiometer antenna points to nadir.

The Amazon's TB difference between the two polarizations is around 1.77 K with a small seasonal variation of 0.4 K (peak-peak). This seasonal variation is opposite to the seasonal variation in Amazon TBs. The mean emissivity of the Amazon are 0.939 and 0.934 for V- and H-polarization, respectively, with a standard deviation of 0.009.

APPENDIX
DERIVATION OF EQUATION (1)

The calibrated antenna temperature T_A' at the radiometer internal calibration plane is given by

$$T_A' = C_r T_{ND} + T_{ref} \tag{A.1}$$

The definitions of the other parameters in the above equation are the same as these in Equation (1).

The internal calibration plane is different from the reference plane for the measured T_A reported in the L1B_TB data file. The relation between them is given by

$$T_A = L_{RF} T_A' - T_{phy,RF}(L_{RF} - 1) \tag{A.2}$$

where $T_{phy,RF}$ is the ambient temperature of the SMAP RF front-end which is between the internal calibration plane and reference plane for the measured T_A.

When corrections are added onto T_{ND} and T_{ref}, the change in the measurement TA is given by

$$\Phi T_A = L_{RF}\left(C_r \delta T_{ND} + \delta T_{ref}\right) \tag{A.3}$$

When a correction, δ_G which is a constant fraction of the antenna gain, is added to the antenna gain, the antenna gain becomes $(1+\delta_G)$G. The expected antenna temperature due to this adjustment is given by

$$\begin{aligned} T'_{A,exp} &= \frac{1}{4\pi}\int_{4\pi}(1+\alpha\delta_G)\cdot G(\Omega)\, T_{B,exp}(\Omega)\, d\Omega \\ &= (1+\delta_G\alpha) T'_{A,exp,0} \end{aligned} \tag{A.4}$$

where $T'_{A,exp,0}$ is the expected antenna temperature using the pre-launch antenna pattern with lossless reflector. δ_G is the gain change in the antenna mainbeam. To maintain the normalization of the antenna pattern, the backlobe with solid angle Ω_3 of the antenna pattern will be scaled by the factor b defined as

$$b = 1 - \delta_G \frac{\int_{\Omega_1} G(\Omega) d\Omega}{\int_{\Omega_3} G(\Omega) d\Omega} \tag{A.5}$$

where Ω_1 is the solid angle of the antenna mainbeam defined as 2.5 times of the 3-dB antenna beamwidth. α is a scale factor which reflects the true antenna temperature change due to the normalization of the antenna pattern after the antenna mainbeam is adjusted, and it's obtained by using simulation.

The expected antenna temperature after considering the reflector loss change is given by

$$T_{A,exp} = \frac{T'_{A,exp}}{L * f_L} + T_{phy,rfl}\left(1 - \frac{1}{L * f_L}\right) \tag{A.6}$$

where f_L is extra loss factor of the reflector, and L is the reflector loss measured before launch. $T_{phy,rfl}$ is the ambient temperature of the reflector.

The difference between the measured TA and expected TA is given by

$$\begin{aligned} \delta T_A &= T_A - T_{A,exp} \\ &= T_{A,0} + L_{RF}\left(C_r \delta T_{ND} + \delta T_{ref}\right) - \left\{\frac{(1+\alpha\delta_G) T'_{A,exp,0}}{L * f_L} + T_{phy,rfl}\left(1 - \frac{1}{L * f_L}\right)\right\} \\ &= \delta T_{A,0} + L_{RF}\left(C_r \delta T_{ND} + \delta T_{ref}\right) \\ &\quad + T_{A,exp,0}\left\{1 - \frac{1+\alpha\delta_G}{f_L}\right\} - \frac{T_{phy,rfl}}{L}\left\{L - \frac{1}{f_L}\right\} \end{aligned} \tag{A.7}$$

where $\delta T_{A,0}$ is the calibration bias before the calibration parameters are adjusted. $T_{A,exp,0}$ is the expected TA with that the pre-launch antenna pattern and reflector loss are used.

If there is any bias in the modeled $T_{A,exp}$ over ocean, the above equation becomes

$$\begin{aligned} \delta T_A &= T_A - \left(T_{A,exp} + B_T\right) \\ &= \delta T_{A,0} + L_{RF}\left(C_r \delta T_{ND} + \delta T_{ref}\right) \end{aligned}$$

$$+T_{A,exp,0}\left\{1-\frac{1+\alpha\delta_G}{f_L}\right\}-\frac{T_{phy,rfl}}{L}\left\{L-\frac{1}{f_L}\right\}-B_T \qquad \text{(A.8)}$$

The goal is to let δT_A converge to zero.

When nadir-looking data are used for the calibration, the solution of the calibration parameters is also needed to let ΔT_A in (A.9) be zero

$$\Delta T_A = \left(T_{A,v}-T_{A,sim,v}\right)-\left(T_{A,h}-T_{A,sim,h}\right) \qquad \text{(A.9)}$$

When the radiometer's internal reference load is used as the hot calibration sources, there will be no correction to its TB (or δT_{ref}=0), then Equation (A.8) becomes

$$\delta T_A = \delta T_{A,0} + L_{RF}C_r\delta T_{ND}$$
$$+T_{A,exp,0}\left\{1-\frac{1+\alpha\delta_G}{f_L}\right\}-\frac{T_{phy,rfl}}{L}\left\{L-\frac{1}{f_L}\right\} \qquad \text{(A.10)}$$

REFERENCES

[1] D. Entekhabi et al., "The Soil Moisture Active Passive (SMAP) Mission," *Proc. IEEE*, vol. 98, no. 5, pp. 704-716, May 2010.

[2] S. Brown, C. Ruf, S. Keihm, and A. Kitiyakara, "Jason microwave radiometer performance and on-orbit calibration," *Marine Geodesy*, vol. 27, no. 1-2, pp. 199-220, 2004.

[3] M. A. Brown, F. Torres, I. Corbella and A. Colliander, "SMOS Calibration," *IEEE Trans. Geosci. Remote Sens.*, vol. 46, no. 3, pp. 646-658, March 2008.

[4] D.M. Le Vine, G.S.E. Lagerloef, F.R. Colomb, S.H. Yueh and F.A. Pellerano, "Aquarius: An Instrument to Monitor Sea Surface Salinity from Space," *IEEE Trans. Geosci. Remote Sens.*, vol. 45, no. 7, pp. 2040-2050, July 2007.

[5] J.R. Piepmeier, P.N. Mohammed, J. Peng, E. Kim, G. De Amici, and C. Ruf, "SMAP L1B Radiometer Half-Orbit Time-Ordered Brightness Temperatures, Version 3," NASA National Snow and Ice Data Center Distributed Active Archive Center, Boulder, Colorado USA, 2015.

[6] C.S. Ruf, S.M. Gross and S. Misra, "RFI Detection and Mitigation for Microwave Radiometry With an Agile Digital Detector," *IEEE Trans. Geosci. Remote Sens.*, vol. 44, no. 3, pp. 694-706, March 2006.

[7] P. N. Mohammed, M. Aksoy, J. R. Piepmeier, J. T. Johnson and A. Bringer, "SMAP L-Band Microwave Radiometer: RFI Mitigation Prelaunch Analysis and First Year On-Orbit Observations," *IEEE Trans. Geosci. Remote Sens.*, vol. 54, no. 10, pp. 6035-6047, Oct. 2016.

[8] J.R. Piepmeier et al, "SMAP L-Band Microwave Radiometer: Instrument Design and First Year on Orbit," *IEEE Trans. Geosci. Remote Sens.*, vol. 55, no. 4, pp. 1954-1966, 2017.

[9] J. Peng et al., "Soil Moisture Active/Passive (SMAP) L-Band Microwave Radiometer Post-Launch Calibration," *IEEE Trans. Geosci. Remote Sens.*, vol. 55, no. 9, pp. 5339-5354, 09 2017.

[10] J. Peng et al., "Soil Moisture Active/Passive (SMAP) L-Band Microwave Radiometer Post-Launch Calibration Upgrade," *IEEE J. Sel. Topics Appl. Earth Obs. Remote Sens.*, vol. 12, no. 6, pp. 1647-1657, 2019.

[11] J. Peng, et al., "SMAP Radiometer Brightness Temperature Calibration for the L1B_TB, L1C_TB (Version 4), and L1C_TB_E (Version 2) Data Products," SMAP Project, Jet Propulsion Laboratory, Pasadena, CA. [Online.], 6 June 2018. [Online]. Available: https://nsidc.org/sites/nsidc.org/files/technical-references/SMAP_L1_Assessment%20Report%2020180601_v9.pdf.

[12] S.H. Yueh, W. Tang, A.G. Fore, G. Neumann, A. Hayashi, A. Freedman, J. Chaubell, and G.S.E. Lagerloef, "L-Band Passive and Active Microwave Geophysical Model Functions of Ocean Surface Winds and Applications to Aquarius Retrieval," *IEEE Trans. Geosc. Remote Sens.*, vol. 51, no. 9, pp. 4619-4632, 2013.

[13] Gabriëlle J. M. De Lannoy, Rolf H. Reichle, and Valentijn R. N. Pauwels, "Global Calibration of the GEOS-5 L-Band Microwave Radiative Transfer Model over Nonfrozen Land Using SMOS Observations," *Journal of Hydrometeorology*, vol. 14, no. 3, pp. 765-785, 01 Jun 2013.

[14] Brown, S., and C. Ruf, "Determination of a Hot Blackbody Reference Target over the Amazon Rainforest for the On-orbit Calibration of Microwave Radiometers," *AMS J. Oceanic Atmos. Tech.*, vol. 22, no. 9, pp. 1340-1352, 2005.

[15] T. Meissner and F. Wentz, "Intercalibration of AMSR-E and WindSat brightness temperature measurements over land scenes," in *2010 IEEE International Geoscience and Remote Sensing Symposium*, Honolulu, HI, 2010.

[16] A.G. Fore; G. Neumann; A.P. Freedman; M.J. Chaubell; W. Tang; A.K. Hayashi; S.H. Yueh, "Aquarius Scatterometer Calibration," *IEEE Journal of Selected Topics in Applied Earth Observations and Remote Sensing*, vol. 8, no. 12, pp. 5424-5432, Dec 2015.